Journal of Applied Polymer Science

Functionalized polyacrylonitrile-nanofiber based immunosensor for *Vibrio cholerae* detection

Pramod K. Gupta,[1,2] A. Gupta,[3] S. R. Dhakate,[3] Zishan H. Khan,[1] Pratima R. Solanki[2]

[1]Department of Applied Sciences and Humanities, Jamia Millia Islamia, New Delhi, India

[2]Special Centre for Nanosciences, Jawaharlal Nehru University, New Delhi, India

[3]Physics and Engineering of Carbon, National Physical Laboratory, New Delhi, India

Correspondence to: P. R. Solanki (E-mail: pratimarsolanki@gmail.com) and Z. H. Khan (E-mail: zishan_hk@yahoo.co.in)

ABSTRACT: Polyacrylonitrile nanofibers (PANnf's) were electrospun directly onto an indium tin oxide (ITO)-coated glass substrate. The PANnf/ITO electrode was partially hydrolyzed with an NaOH aqueous solution at ambient temperature to convert the nitrile groups of the PANnf's into carboxyl groups was confirmed by Fourier transform infrared spectroscopy. Furthermore, 1-ethyl-3-(3-dimethylaminopropyl) carbodiimide–*N*-hydroxy succinimide chemistry was used to activate the —COOH groups of PANnf's for the covalent co-immobilization of monoclonal antibodies against *Vibrio cholerae* and bovine serum albumin for *V. cholerae* toxin detection. Structural, functional, and electrochemical studies of the PANnf/ITO electrode and BSA/Ab/PANnf/ITO immunoelectrode were performed, and found a uniform distribution of nanofibers with diameter of 325 ± 7.7% nm. The electrochemical response studies showed an improved sensing performance of the immunoelectrode with a detection of 6.25–500 ng/mL, a low limit of detection of 0.22 ng/mL, a sensitivity of 90 nA ng^{-1} mL cm^{-2}, an association constant of 45.2 ng/mL, and a dissociation constant of 8 ng/mL.
 J. Appl. Polym. Sci. **2016**, *133*, 44170.

KEYWORDS: biomedical applications; electrospinning; nano fibers; *Vibrio cholerae*

Received 11 March 2016; accepted 6 July 2016

DOI: 10.1002/app.44170

INTRODUCTION

Recently, polymer nanofibers (one-dimensional materials) have emerged as promising candidates because of their high surface area, excellent mechanical properties, and porosity. These unique properties of nanofibers ensure their potential applications in the fields of biomedical applications, water purification, catalysis, protective clothing, reinforcement, nanobioelectronics, and optical devices.[1–6] Polymer nanofibers can be produced by vapor growth, templates, drawing, self-assembly, and spinning methods such as melt spinning and wet spinning.[7–9] However, the electrospinning technique has been widely explored as a simple and easy way to prepare continuous fibers with large surface-to-volume ratios and its flexibility in controlling the fiber diameter from the micrometer to the nanometer scale under mild conditions.[10] The electrospinning technique works on the principle of electrostatic forces between the anode and cathode terminals. The morphology of the electrospun nanofiber can be controlled by the applied voltage, polymer molecular weight, experimental design, viscosity, conductivity, and concentration of the solution.[11,12] Polymer nanofibers synthesis and morphology also depend on the tip-to-collector distance, collector speed, flow rate, and surface tension of the feed solution. Increases in the distance and collector speed causes an increase in the polymer stretching and results in thinner fibers. An increase in the flow rate reduces the stretching and also causes bead formation in the nanofibers.[13,14] Electrospinning techniques provide randomly oriented nanofiber mats and uniform, highly oriented fibers and require a minimum polymer concentration for the formation of continuous fibers rather than droplets. In the past several decades, a variety of polymers, such as engineering plastics, biopolymers, conducting polymers, and polymer blends, has been successfully electrospun into nanofibers from an electrically charged jet of polymer solution.[15,16]

Among the various studied polymers, polyacrylonitrile nanofibers (PANnf's) have received significant attention because of their unique features, including their higher carbon yield, excellent solubility, higher mechanical properties, and higher thermal stability.[17] Polyacrylonitrile (PAN) polymer is soluble in aprotic solvents, such as dimethylformamide (DMF),

Additional Supporting Information may be found in the online version of this article

dimethylacetamide, and dimethyl sulfoxide, but completely soluble in DMF at a high concentration.[18] In a previous article,[19] we reported that the effect of concentrations ranging from 7.5 to 12% w/w on the synthesis of PAN copolymer. Nanofibers synthesized with electrospinning are low cost, continuous, and easy to align and assemble, and they are used in many applications, such as wound dressings, filtration, drug delivery, reinforcement, catalysis, electronic and optical devices, and biomedical and pharmaceutical applications.[14,20] The nitrile group on PANnf's can easily be modified into a carboxyl group; this enhances the interaction between biomolecules and nanofibers. Zhang *et al.*[21] have reported a study of the poly(acrylonitrile-*co*-methyl methacrylate) plasticized with $LiBF_4$ as a gel polymer electrolyte for Li-ion cells. They used β-galactosidase on amino-functionalized electrospun poly(acrylonitrile-*co*-methyl methacrylate) nanofibers with glutaraldehyde[1]; the polymer showed better resistance to higher temperature (65 °C) and higher pH (11.0) and improved stability compared to one with a free form of the enzyme and retained the enzyme activity (64%).[22,23] The network of these nanofibers could be used directly as an electrode after stabilization;[24] these nanofibers had the advantage of a high reproducibility, low noise, and high reliability for biosensor applications. Recently, Babakhanian *et al.*[25] have reported the electrospinning of a Lake Red C (LRC) pigment doped PAN based electrochemical sensor for aflatoxin B1 detection. With this in mind, we report the fabrication of PANnf's and the development of an immunosensor.

Vibrio cholerae is a comma-shaped gram-negative pathogenic bacterium, which causes diarrheal infection in human beings. During infections, it secretes the cholera toxin, and this leads to a high mortality.[26] Thus, the detection of this *V. cholerae* toxin B is important; it requires a rapid, sensitive, and effective analytical tool such as an immunosensor. During last few years, immunosensors based on different nanostructured materials for the detection of *Vc*T have been reported.[27–33] Table S1 in the Supporting Information shows the biosensing response of these electrodes. Arshak *et al.*[34] have reported a polyaniline grafted on a lignin-based sensing platform for the detection of foodborne pathogens, including *Salmonella* species, *Bacillus cereus*, and *Vibrio parahaemolyticus* without antibodies (Abs) and monitored changes in the resistance after the interaction of bacteria with the sensor. This sensor had limitations of specificity and sensitivity.

The aim of this study was to develop a novel architecture for the development of a PANnf-based electrochemical immunosensor for the detection of *V. cholerae*, with the objectives of a high sensitivity, selectivity, low cost, and easy miniaturization. Here, we had electrospun PANnf's directly deposited onto an indium tin oxide (ITO)-coated glass substrate to fabricate an electrochemical immunosensor. The nitrile groups of the PANnf's were converted into carboxyl groups and used for the covalent immobilization of monoclonal Abs specific to *V. cholerae*, and the detection of *Vc*T was carried out with the Differential Pulse Voltammetry (DPV) technique. To the best of our knowledge, this is the first report on a PANnf-based immunosensor for pathogen (*V. cholerae*) detection.

EXPERIMENTAL

For the fabrication of nanofibers, we used PAN (94%)–methyl methacrylate (6%) as a source material (R. K. Industries, United Kingdom). DMF, with a purity of 99%, and phosphate-buffer (PB; pH 7.0) were procured from Thermo Fisher Scientific Pvt., Ltd. (India). The ITO-coated glass substrate, with a thickness of 1.1 mm, a sheet resistance of 25 Ω/square, and a transmittance of 90%, was imported from Balzers (United Kingdom, Baltracom 247 ITO). Biomolecules as monoclonal Abs specific to *V. cholerae*, *V. cholerae* toxin B (*Vc*T) as an antigen, and bovine serum albumin (BSA) were purchased from M/s Genetix Biotech Asia. All of the chemicals used in this experiment were analytical grade and were used without further purification.

Fabrication of the PANnf's on the ITO Surface

We have fabricated PANnf/ITO electrodes through the electrospinning of PANnf's directly on the ITO substrate as a collector. The PAN microfibers were chopped and dispersed in DMF at a concentration of 10 wt % with ultrasonication for 2 h. The well-dispersed solution of PAN microfibers was stirred with a magnetic stirrer for 10–12 h to obtain a transparent homogeneous solution.[35] The homogeneous solution of PAN microfibers was then electrospun into the PANnf's onto the ITO substrate (0.5 × 0.5 cm) at a voltage of 15 kV and a flow rate of 0.2 mL/h. The tip-to-collector distance was kept at 20 cm, and the collector speed as 2000 ± 50 rpm. The electrospinning was performed at room temperature (25 °C) and a humidity of 30%. Before the electrospinning processes, the ITO electrodes were ultrasonically cleaned in a solution containing H_2O_2, NH_4OH, and H_2O at a ratio of 1:1:5; this was followed by two washings with deionized water. All of the electrodes were fabricated at room temperature (25 °C).

Functionalization of the PANnf/ITO Electrode

For the functionalization, the PANnf/ITO electrode was partially hydrolyzed with a 2 *M* NaOH solution for 1 h at 40 °C. The partial hybridization of PANnf/ITO generated functional carboxyl (COO) groups on the electrode surface with some of the amine (NH_2) groups. During this process, the nitrile (—CN) groups on the surface of the PANnf's were partially converted into carboxyl and amine groups[1,36] (Scheme 1). Afterward, the functionalized PANnf/ITO electrode was exposed to 10 μL of the crosslinking agents 1-ethyl-3-(3-dimethylaminopropyl) carbodiimide (EDC) and *N*-hydroxy succinimide (NHS) at a ratio of 1:1 to activate the carboxyl groups of PANnf's. EDC–NHS chemistry was used to couple the carboxyl groups of the PANnf's to the amine groups of Abs, in which EDC (0.4 *M*) acted as a coupling agent and NHS (0.1 M) acted as an activator.[37]

Immobilization of Abs and BSA onto the PANnf/ITO Electrodes

To immobilize the Abs onto the carboxyl-functionalized group of the PANnf electrode, we were prepared a fresh two-stock solution with a concentration of 0.01 mg/mL in phosphate buffer (pH 7.0, 50 m*M*). Then, 10 μL of an Ab stock solution was loaded onto the carboxyl-functionalized group of the PANnf electrode surface and kept in a humid chamber for 6 h at room temperature (25 °C). The functionalized carboxyl group of the PANnf's and the —NH_2 terminal of an Ab was linked with each

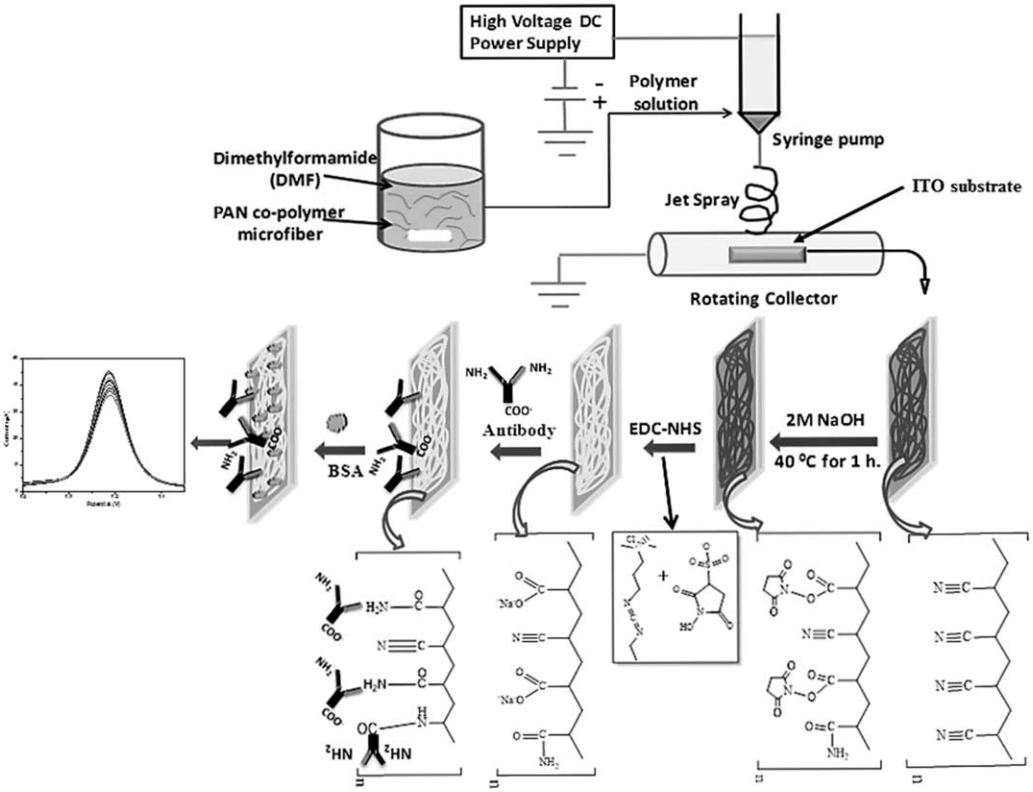

Scheme 1. Stepwise fabrication of the electrospinning-based BSA/Ab/PANnf/ITO immunoelectrode. DC = direct current.

other by the establishment of C—N bonding (Scheme 1). Furthermore, the carboxyl (COOH) terminal of some Abs was attached with the partially generated amine (NH_2) groups of the PANnf's. Afterward, this electrode was washed with phosphate buffer (pH 7.0, 50 m*M*) to remove the unbounded Abs from the Ab/PANnf/ITO immunoelectrode surface. Furthermore, 10 µL of BSA (0.01 mg/mL) was loaded onto the electrode surface and left for 4 h to block the unspecific sites present on the immunoelectrode surface. This fabricated BSA/Ab/PANnf/ITO immunoelectrode was stored at 4 °C when not in use. To examine the sensitivity of the fabricated immunoelectrode for *Vc*T, we prepared solutions with different concentrations of *Vc*T, which varied from 6.25 to 500 ng/mL in phosphate buffer (50 m*M*, pH 7.0).

Characterization Techniques

The PANnf/ITO electrode, fabricated with an electrospinning instrument (ESPIN-NANO), was procured from PECO (Chennai, India). The crystallization characteristics of the PANnf's were investigated with an X-ray diffractometer (PANalytical X'Pert PRO 2200 diffractometer with Cu Kα radiation at λ = 1.5406 Å). The surface morphologies of the PANnf/ITO and Ab/PANnf/ITO immunoelectrode were investigated with scanning electron microscopy (EVO 40, Zeiss). The Fourier transform infrared (FTIR) spectroscopy (Varian 7000 FT) was used to monitor the modification of the PANnf electrode with NaOH, Abs, and BSA, respectively. Electrochemical studies were conducted with an Autolab potentiostat/galvanostat (Eco Chemie, The Netherlands) with a three-electrode cell working electrode, platinum wire as the auxiliary electrode, and Ag/AgCl as the reference electrode in saline PB (PBS, pH 7.0, 0.9% KCl) containing 3.3 m*M* $[Fe(CN)_6]^{3-/4-}$.

RESULTS AND DISCUSSION

Characterization Studies

Figure 1 shows the X-ray diffraction pattern of the PANnf's, which showed a crystalline nature. The diffraction pattern exhibited major peaks at 2θs of 14.1, 16.7, and 25.5°. The prominent peak appeared at 16.7°, and a small peak at 25.5° was assigned to the PAN, whereas the peak at 14.1°

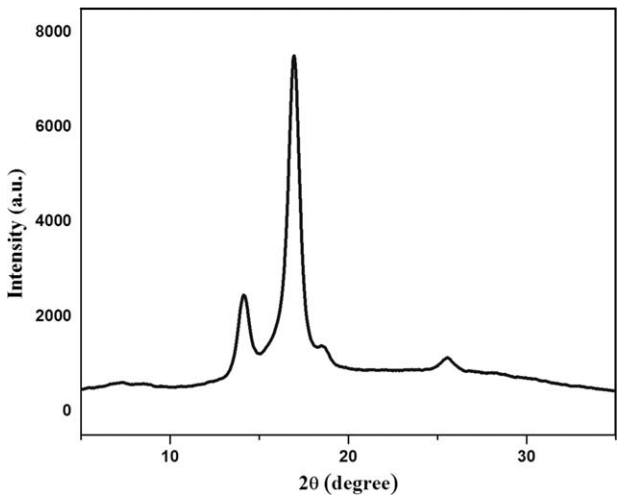

Figure 1. X-ray diffraction pattern of the PANnf copolymer.

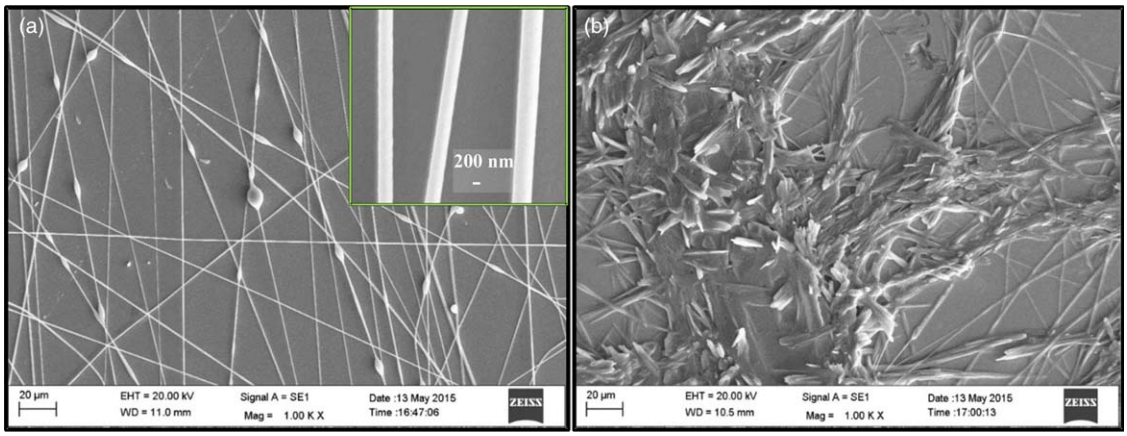

Figure 2. Scanning electron microscopy images of the (a) PANnf/ITO and (b) Ab/PANnf/ITO immunoelectrode. [Color figure can be viewed in the online issue, which is available at wileyonlinelibrary.com.]

corresponded to methyl methacrylate.[38,39] These results indicate that nanofibers made up of PAN–methyl methacrylate (with 6% methyl methacrylate) as a source material without any solvent impurities.

To investigate the surface morphology of the PANnf/ITO and Ab-modified Ab/PANnf/ITO immunoelectrode, scanning electron microscopy analysis was carried out (Figure 2). It is clear from Figure 2(a) that the nanofibers formed were mostly semi-aligned, uniform, and randomly distributed on the surface of the ITO; this created a network of the polymeric chain. The networking of these nanofibers provided a good accessible platform for the biomolecules for a better electrochemical response. The diameter of nanofibers was found to be 325 ± 7.7% nm [inset in Figure 2(a)]. However, after the immobilization of Ab, the PANnf/ITO electrode exhibited dense networking; this indicated that the Abs were interconnected with the nanofibers (Figure 2b).

Figure 3(a–c) shows the FTIR spectra of the PANnf/ITO electrode, functionalized PANnf/ITO electrode, and Ab/PANnf/ITO immunoelectrode. The IR spectra of the PANnf's (curve a) showed characteristic absorbance peaks at 1730, 2243, and 2934 cm^{-1}; the peaks at 1730 and 2243 cm^{-1} correspond to C═O whereas peak at 2934 cm^{-1} to C═H stretching. The peak observed at 2243 cm^{-1} was assigned to the nitrile groups of the PAN chain.[40] After the functionalization of PANnf's with NaOH (curve b), all of the absorption peaks observed were same as in the spectra for PANnf's (curve a). However, the new peak at 1580 cm^{-1} was assigned to the carboxyl groups (specified in the inset of Figure 3). The results confirm the conversion of nitrile groups into carboxyl groups because of the partial hydrolyzation of PANnf's, which are more susceptible to the alkaline conditions.[35,41] After the immobilization of Abs on the functionalized PANnf surface (curve c), the broad peaks observed at 1675and 2951 cm^{-1} were assigned to C═O stretching correspond to primary amides and ─CH_2 aliphatic compounds.[42,43] This confirmed the successful immobilization of Abs on the PANnf/ITO electrode surface.

The electrochemical characterization of ITO, PANnf/ITO, Ab/PANnf/ITO, and BSA/Ab/PANnf/ITO was carried out with a DPV technique in PBS containing $[Fe(CN)_6]^{3-/4-}$ in the potential range −0.2 to 0.6 V; at a step potential of 5 mV with a time interval of 0.5 ms [Figure 4(A-a–d)]. We observed that the magnitude of the final current - initial current (ΔI) of the PANnf/ITO electrode (53 µA) decreased compared to that of the bare ITO (59 µA); this may be due to the lower conductivity of the nanofibers with respect to ITO. After the immobilization of Abs onto the PANnf/ITO surface, the magnitude of the current peak further decreased (44 µA); this revealed the slower electron transfer between the electrode and electrolyte due to Ab immobilization on the PANnf/ITO electrode surface. After the immobilization of macromolecule size BSA onto the Ab/PANnf/ITO immunoelectrode, further the current decreased to a value of 34 µA. This indicated that due to the insulating nature, BSA inhibited the flow of electron.

The cyclic voltammetry of the PANnf/ITO and BSA/Ab/PANnf/ITO immunoelectrode performed as a function of the scan rate (ν), which was varied from 10 to 100 mV/s in PBS containing $[Fe(CN)_6]^{3-/4-}$ [Figure 4(B-a,b)]. It has been observed that the cathodic peak current (I_c) and the anodic peak current (I_a) increased linearly (linear regression constant = 0.99) with

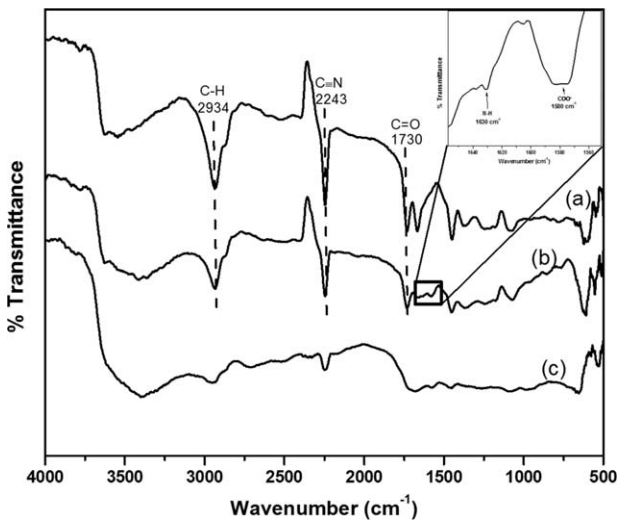

Figure 3. FTIR spectrum of (a) PANnf/ITO, (b) the PANnf/ITO electrode functionalized with NaOH, and (c) the Ab/PANnf/ITO electrode.

increasing square root of scan rate (v) for both electrodes [insets in Figure 4B(a,b)]. This revealed the presence of quasi-reversible behavior.[44] The anodic peak potential shifted toward the positive side and the cathodic peak potential shifted toward the negative side with increasing v; this indicated the existence of a diffusion-controlled process.[25] The slopes and intercepts were estimated with eqs. (1) and (2):

$$I_{pa}(\mu A)\text{PANnf/ITO} = 0.084\ \mu\text{A} + 0.095\ \frac{\mu\text{A mV}}{\text{s}} \times v\left(\frac{\text{mV}}{\text{s}}\right)^{\frac{1}{2}} \quad (1)$$

$$\text{with } R^2 = 0.99$$

$$I_{pa}(\mu A)\text{BSA/Ab/PANnf/ITO} = 0.216\ \mu\text{A} + 0.297\ \frac{\mu\text{A mV}}{\text{s}} \quad (2)$$

$$\times v\left(\frac{\text{mV}}{\text{s}}\right)^{\frac{1}{2}} \text{ with } R^2 = 0.99$$

With the Randles–Sevcik equation,[45] the value of the diffusion coefficient (D) was calculated for the diffusion of $[Fe(CN)_6]^{3-/4-}$ from an electrolyte solution to the respective electrode surface:

$$I_p = (2.69 \times 10^5) n^{\frac{3}{2}} A D^{\frac{1}{2}} C v^{\frac{1}{2}} \quad (3)$$

where I_{pa} is the anodic peak current, n is the number of electrons involved or the electron stoichiometry($n = 1$), A is the surface area of the electrode (0.25 cm^2), C is the ferro/ferry concentration (3.3 mM), and v is 50 mV/s. The D values of the PANnf/ITO and BSA/Ab/PANnf/ITO immunoelectrode were found to be 1.66×10^{-12} and 1.50×10^{-12} cm^2 s^{-1}, respectively. The higher value of D for the PANnf/ITO electrode may have been due to the better conductive nature of the electrode compared to that of the Ab/PANnf/ITO electrode.

The surface concentrations of the ionic species for the PANnf/ITO and BSA/Ab/PANnf/ITO electrodes in the presence of PBS with the ferry/ferricyanide redox probe were estimated from the current versus potential plot with the Brown–Anson model[45] as per eq. (4):

$$I_p = \frac{n^2 F^2 I^* A v}{4RT} \quad (4)$$

where F is the Faraday constant (96,485 C/mol), I^* is the surface concentration of PANnf/ITO and BSA/Ab/PANnf/ITO immunoelectrodes (mol/cm^2), v is 50 mV/s, R is the gas constant (8.314 J mol^{-1} K^{-1}), and T is the room's temperature (300 K). The values of the surface concentrations for the PANnf/ITO, Ab/PANnf/ITO, and BSA/Ab/PANnf/ITO immunoelectrodes were estimated to be 1.05×10^{-8}, 1.02×10^{-8}, and 1.00×10^{-8} mol/cm^2, respectively.

The electrochemical surface area (A_e) was calculated by the insertion of the value of the diffusion constant into the Randles–Sevcik equation[46]:

$$A_e = \frac{S}{2.99 \times 10^5} n^{\frac{3}{2}} C D^{\frac{1}{2}} \quad (5)$$

where S is the slope obtained from the linear regression of I_p versus $n^{1/2}$. The A_e values of the PANnf/ITO and BSA/Ab/PANnf/ITO immunoelectrodes were found to be 1.40 and 1.35 mm^2, respectively.

The reversibility of the electron-transfer kinetics did not depend on v, but it also depended on the standard heterogeneous electron-transfer rate constant (K_s). With the Laviron model[46] [as given in eq. (9)], the estimated values of K_s for the PANnf/ITO and BSA/Ab/PANnf/ITO immunoelectrodes were 0.84 and 0.41 s^{-1}, respectively. The high value of K_s for the PANnf/ITO electrode indicated a fast electron exchange between the electrode surface and redox species in the electrolyte:

$$K_s = mnFv/RT \quad (6)$$

where m is the peak-to-peak separation of potentials (V).

Figure 4(C) shows the electrochemical impedance spectra (EIS) of the ITO substrate [curve 4(a)], PANnf/ITO [curve 4(b)], Ab/PANnf/ITO [curve 4(d)], and BSA/Ab/PANnf/ITO [Figure 4(d)] immunoelectrodes, which were studied in PBS containing $[Fe(CN)_6]^{3-/4-}$ in the frequency range 0.00–10^5 Hz at zero potential. On the basis of the electrochemical impedance spectra, we evaluated the charge-transfer resistance (R_{CT}) and double-layer capacitance (C_{dl}) at the electrode/electrolyte interface. The change in the value of R_{CT} for the different electrode depended on the electrode/electrolyte interface occurred during the electrochemical measurement. Figure 4(C) shows the Nyquist plots of the respective electrodes; to investigate the relative changes in electrodes in terms of the R_{CT}, the constant-phase element at the electrode/electrolyte interface, and K_s.[47] Here, the value of R_{CT} was equal to the diameter of the Nyquist plot, and this varied with the modification of the PANnf/ITO electrode with respective biomolecules (Ab and BSA) onto the surface of the electrode.

The Nyquist plot of the impedance for a parallel RC circuit (the equivalent of a Randles circuit) consists of the real impedance (Z') and imaginary impedance (Z'') obtained at different frequencies. R_{CT} and C_{dl} were evaluated from a Nyquist plot with eqs. (7) and (8), as follows:

$$Z(\omega) = Z' + JZ = R_s + \frac{R_\rho}{(1 + J\omega C_{dl})} \quad (7)$$

$$Z' = R_s + \frac{R_\rho}{(1 + \omega R_\rho^2 C_{dl}^2)} \text{ and } -Z'' = \frac{\omega R_\rho^2 C_{dl}}{(1 + \omega R_\rho^2 C_{dl}^2)} \quad (8)$$

where R_s and R_p = R_{CT} denote the electrolyte and polarization resistances, respectively, obtained at zero potential.[48]

A significant change in the value of R_{CT} (curve b; 5.21 kΩ) for the PANnf/ITO electrode as compared to the bare ITO (curve a; 3.92 kΩ) has observed. This revealed that the PANnf/ITO electrode enhanced R_{CT} of the redox probe toward the electrode from the electrolyte. In addition, this indicated that the PANnf had proximity to the ITO surface. After the immobilization of Abs onto the PANnf surface, the R_{CT} (curve c; 5.50 kΩ) value increased. This may have been due to the formation of an insulating layer of Abs on the PANnf/ITO electrode; this resulted in an inhibition of the flow of electrons generated by redox species and enhanced the impedance. After the modification of the Ab/PANnf/ITO immunoelectrode with BSA, the value of R_{CT} (curve

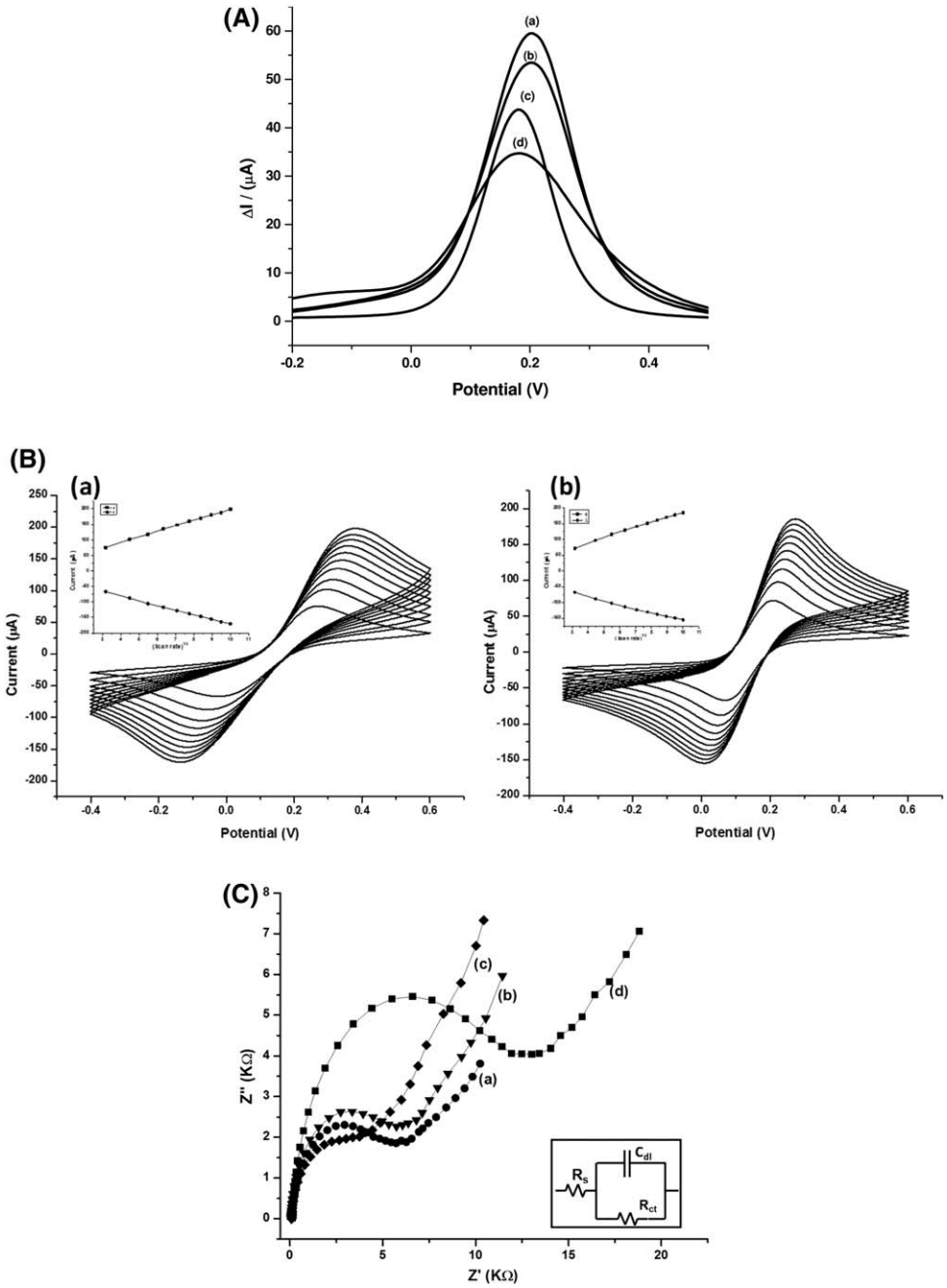

Figure 4. (A) DPV of (a) ITO, (b) PANnf/ITO, (c) Ab/PANnf/ITO, and (d) the BSA/Ab/PANnf/ITO immunoelectrode. (B) Cyclic Voltammetry (CV) of (a) PANnf/ITO and (b) the BSA/Ab/PANnf/ITO immunoelectrode as a function of v from 10 to 100 mV/s. The inset displays a graph of the current versus the square root of v. (C) Frequency response analysis (FRA) of (a) ITO, (b) PANnf/ITO, (c) Ab/PANnf/ITO, and (d) the BSA/Ab/PANnf/ITO immunoelectrode at a zero potential in the frequency range of 0.1–10^5 Hz.

d; 10.67) increased further; this suggested that BSA covered the available nonspecific active sites on the Ab/PANnf/ITO immunoelectrode because BSA had an insulating nature that caused steric hindrance for the electrons during the $[Fe(CN)_6]^{3-/4-}$ redox reaction.

Other kinetic parameters, such as K_e and the time constant (t), of the BSA/Ab/PANnf/ITO immunoelectrode were evaluated to investigate the interfacial interactions of the biomolecules at the electrode/electrolyte interface. The K_e and t values of the PANnf/ITO electrode were calculated before and after the Ab immobilization with the following relation:

$$K_e = \frac{RT}{n^2 R_{CT} A C F^2} \quad (9)$$

The value of rate constant (K_e) of the PANnf/ITO and Ab/PANnf/ITO immunoelectrode were obtained as 6.23×10^{-5} and

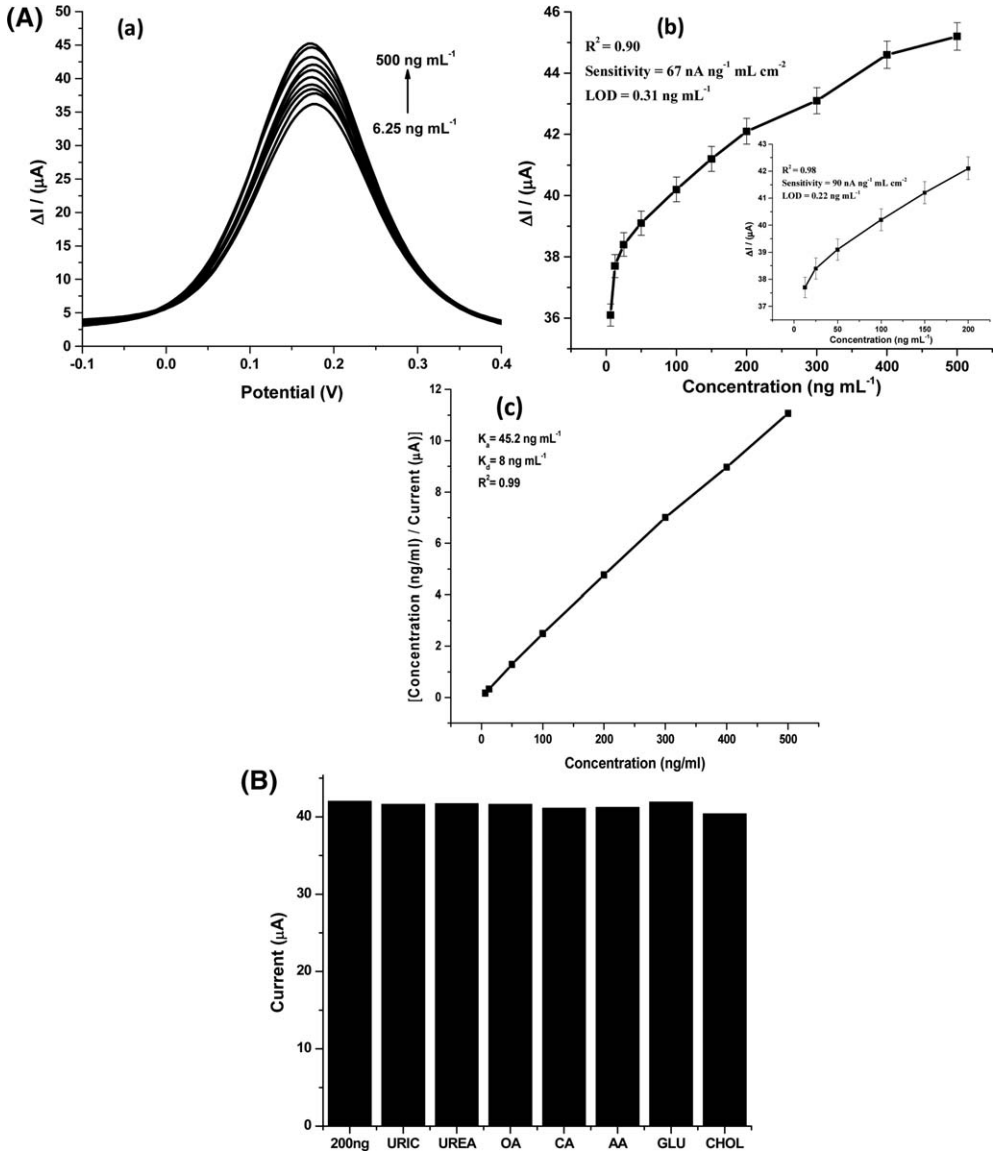

Figure 5. (A) (a) DPV response studies of BSA/Ab/PANnf/ITO immunoelectrode as a function of the antigen concentration (6.25–500 ng/mL), (b) plot of the response versus the antigen concentration, and (c) Hanes–Wolf plot the antigen concentration versus the antigen concentration/current. (B) Effect of interferents on the response of the BSA/Ab/PANnf/ITO immunoelectrode. AA = acetic acid; CHOL = cholesterol; GLU, glucose; OA, oxalic acid; CA, citric acid.

5.90×10^{-5}, respectively. The lower value corresponded to the immunoelectrode and indicated a slow electron exchange between the redox probes and the electrode. However, BSA immobilized on the Ab/PANnf/ITO immunoelectrode provided resistance to the electron transfer; this resulted in a decreased electron-transfer rate constant (3.04×10^{-5}) and, subsequently, a low generated capacitance at the electrode surface.

The observed high value of t for the BSA/Ab/PANnf/ITO immunoelectrode (0.018 ms) compared to those of the Ab/PANnf/ITO immunoelectrode (0.013 ms) and PANnf/ITO electrode (0.012) was due to the slow diffusion of $[Fe(CN)_6]^{3-/4-}$ ions at the electrode/electrolyte interface t was associated with a frequency at which the maximum impedance was obtained (f_{max}), and R_{CT} has been calculated with the C_{dl} value via eq. (10):

$$R_{CT} C_{dl} = 1/(2\pi f_{max}) = t \quad (10)$$

where R_{CT} is the charge transfer resistance or polarization resistance.

Electrochemical Response Studies

The electrochemical response of the BSA/Ab/PANnf/ITO immunoelectrode was investigated as a function of the *Vc*T concentration (6.25–500 ng/mL) with DPV in PBS containing $[Fe(CN)_6]^{3-/4-}$ at zero potential. During the electrochemical measurements, the BSA/Ab-/PANnf/ITO immunoelectrode was treated with 10 μL of *Vc*T and incubated for about 5 min at 25 °C. We found that the magnitude of the current increased with increasing *Vc*T concentration. This increase in the magnitude of the current revealed the formation of an antigen–Ab

complex by probing the features of the interfacial properties; the complex acted as an electron-transfer accelerating layer for redox species on the immunoelectrode surface.[49] Moreover, this might have been due to the fact that when *Vc*T interacted with the Ab/PANnf/ITO immunoelectrode, the resulting surface charge of the immunoelectrode became quite different from that of the individual Ab or *Vc*T. This change in the surface energy was related to the electrochemical response.[50] This BSA/Ab/PANnf/ITO immunosensor displayed a linear response to *Vc*T in the concentration range 6.25–500 ng/mL with the following linear equation and a sensitivity of 67 nA ng^{-1} mL cm^{-2} and a low limit of detection (LOD) of 0.31 ng/mL:

$$\Delta I\ (\mu A) = 0.0167 \times \text{Concentration}\ (ng/mL) + 37.65$$

A more linear (correlation coefficient = 0.98) increase in currents corresponding to the *Vc*T concentration was observed within the range 12.5–200 ng/mL; this gave a sensitivity of 90 nA ng^{-1} mL cm^{-2}, an LOD of 0.22 ng/mL, and the linear equation [inset of Figure 5A(a, b)]:

$$\Delta I(\mu A) = 0.0226 \times \text{Concentration}\ (ng/mL) + 37.59$$

It is found that the BSA/Ab/PANnf/ITO immunosensor showed a wide detection range compared to previous values reported in literature. A comparison of this study with previously reported works is presented in Table S1 (Supporting Information). Furthermore, the values of the association constant (K_a) and disassociation constant (K_d) for the BSA/Ab/PANnf/ITO immunoelectrode were estimated with the Hanes–Wolf plot [graph between the antigen concentration and the antigen concentration divided by the current,[51,52] Figure 5A(c)]. The inverse value of the slope observed by the linear fitting of the Hanes–Wolf plot gave a value of K_a of 45.2 ng/mL, whereas the product of the K_a and intercept gave a value of K_d of 8 ng/mL. The small value of K_a indicated an increased affinity in the immobilized Abs of the BSA/Ab/PANnf/ITO immunoelectrode toward the antigen.

Repeatability and Reproducibility

The repeatability of the BSA/Ab/PANnf/ITO immunosensor was investigated by the measurement of the DPV responses for a specific concentration (100 ng/mL) of *Vc*T. For successive measurements (six times), the value of the relative standard deviation was observed to be 2.12%. To investigate the reproducibility of the immunosensor, six BSA/Ab/PANnf/ITO immunoelectrodes were fabricated, and their DPV response was observed independently. The estimated value of the relative standard deviation with an acceptable variation coefficient of 3.48% was observed. The results of the repeatability and reproducibility experiments performed on BSA/Ab/PANnf/ITO immunoelectrode were satisfactory (Supporting Information, Figure S1). The successful immobilization of Abs implied the repeatability and reproducibility of the immunosensor.

The relative standard deviation was calculated with the following equation:

$$\text{Relative standard deviation}\ (\%) = (\text{Standard deviation/Average}) \times 100$$

Selectivity

The selectivity of the BSA/Ab/PANnf/ITO immunosensor was studied in the presence of different analytes, including uric acid (0.5 m*M*), urea (0.8 m*M*), oxalic acid (1 m*M*), acetic acid (0.1 m*M*), glucose (4 m*M*), and cholesterol [4 m*M;* Figure 5(b)]. During the measurements, we mixed the same volume (10 µL) of desired interference with a fixed antigen concentration (200 ng/mL) and observed an electrochemical response after an incubation time of 5 min. We found that there was no significant change in the magnitude of the current after the interaction of the BSA/Ab/PANnf/ITO immunoelectrode with interfering compounds.

CONCLUSIONS

A successful immobilization of Abs (specific to *Vc*T) on the functionalized surface of a PANnf/ITO electrode via covalent immobilization was accomplished. The as-fabricated BSA/Ab/PANnf/ITO immunoelectrode gained improved detection of *Vc*T in the detection ranges 6.25–500 ng/mL, with an LOD of 0.22 ng/mL and a sensitivity of 90 nA ng^{-1} mL cm^{-2} with the DPV technique. The small value of K_a revealed an increase in the affinity of the immobilized Abs of the BSA/Ab/PANnf/ITO immunoelectrode toward the antigen. The presence of interferents, such as glucose, uric acid, urea, oxalic acid, acetic acid, cholesterol, and ascorbic acid, did not significantly affect the specificity of the immunoelectrode toward *Vc*T detection. We expected that the as-fabricated PANnf-based immunosensor may find applications in the field of biomedical science.

ACKNOWLEDGMENTS

The authors are thankful to the Advanced Instrumentation Research Facility of Jawaharlal Nehru University for the instrumentation facilities. Pramod K. Gupta thanks the University Grants Commission for its financial support through a junior research fellowship. This work was supported by a grant from the Department of Science and Technology of the Government of India and the University Grants Commission India (Universities with Potential for Excellence II; project 58).

REFERENCES

1. Wang, Z.-G.; Wan, L.-S.; Xu, Z.-K. J. *Membr. Sci.* **2007**, *304*, 8.
2. Liu, Z.; Zhou, C.; Zheng, B.; Qian, L.; Mo, Y.; Luo, F.; Shi, Y.; Choi, M. M.; Xiao, D. *Analyst* **2011**, *136*, 4545.
3. Zhang, L.; Luo, J.; Menkhaus, T. J.; Varadaraju, H.; Sun, Y.; Fong, H. J. *Membr. Sci.* **2011**, *369*, 499.
4. Dissanayake, M.; Bandara, L.; Bokalawala, R.; Jayathilaka, P.; Ileperuma, O.; Somasundaram, S. *Mater. Res. Bull.* **2002**, *37*, 867.
5. Liu, H.; Hsieh, Y. L. *Macromol. Rapid Commun.* **2006**, *27*, 142.
6. Zheng, H.; Xue, H.; Zhang, Y.; Shen, Z. *Biosensors Bioelectron.* **2002**, *17*, 541.
7. Zhang, L. *Int. J. Nano Stud. Technol.* **2014**, *3*, 01.

8. Zhang, L.; Aboagye, A.; Kelkar, A.; Lai, C.; Fong, H. J. *Mater. Sci.* **2014**, *49*, 463.
9. Gupta, A.; Dhakate, S. Electrospinning: Practical Approach to Nanofibers, New Era of Research, Lap Lambert Academic: Saarbrücken, Germany, 2012.
10. Fennessey, S. F.; Farris, R. J. *Polymer* **2004**, *45*, 4217.
11. Moon, S.; Choi, J.; Farris, R. J. J. *Appl. Polym. Sci.* **2008**, *109*, 691.
12. Li, Z.; Wang, C. One-Dimensional Nanostructures; Springer Berlin Heidelberg, **2013**, 15.
13. Beachley, V.; Wen, X. *Mater. Sci. Eng. C* **2009**, *29*, 663.
14. Jalili, R.; Morshed, M.; Ravandi, S. A. H. *J. Appl. Polym. Sci.* **2006**, *101*, 4350.
15. Huang, Z.-M.; Zhang, Y.-Z.; Kotaki, M.; Ramakrishna, S. *Compos. Sci. Technol.* **2003**, *63*, 2223.
16. Khalil, H. A.; Bhat, A.; Yusra, A. I. *Carbohydr. Polym.* **2012**, *87*, 963.
17. Raza, A.; Wang, J.; Yang, S.; Si, Y.; Ding, B. *Carbon Lett.* **2014**, *15*, 1.
18. Iovleva, M.; Smirnova, V.; Budnitskii, G. *Fiber Chem.* **2001**, *33*, 262.
19. Dhakate, S. R.; Gupta, A.; Chaudhari, A.; Tawale, J.; Mathur, R. B. *Synth. Met.* **2011**, *161*, 411.
20. Nataraj, S.; Yang, K.; Aminabhavi, T. *Prog. Polym. Sci.* **2012**, *37*, 487.
21. Zhang, S.; Xu, K.; Jow, T. *Solid State Ionics* **2003**, *158*, 375.
22. El-Aassar, M. J. *Mol. Catal. B* **2013**, *85*, 140.
23. El-Aassar, M.; Al-Deyab, S. S.; Kenawy, E. R. *J. Appl. Polym. Sci.* **2013**, *127*, 1873.
24. Doshi, J.; Reneker, D. H. In Industry Applications Society Annual Meeting, 1993, Conference Record of the 1993 IEEE; IEEE: Toronto, **1993**; p 1698; Vol. *3*.
25. Babakhanian, A.; Momeneh, T.; Aberoomand-azar, P.; Kaki, S.; Torki, M.; Kiaie, S. H.; Sadeghi, E.; Dabirian, F. *Analyst* **2015**, *140*, 7761.
26. Ali, M.; Lopez, A. L.; You, Y.; Kim, Y. E.; Sah, B.; Maskery, B.; Clemens, J. *Bull. World Health Org.* **2012**, *90*, 209.
27. Loyprasert, S.; Hedström, M.; Thavarungkul, P.; Kanatharana, P.; Mattiasson, B. *Biosensors Bioelectron.* **2010**, *25*, 1977.
28. Chiriac, M. S.; Ionescu, R. E. *Lab Chip* **2011**, *11*, 658.
29. Rao, V. K.; Sharma, M. K.; Goel, A. K.; Singh, L.; Sekhar, K. *Anal. Sci.* **2006**, *22*, 1207.
30. Solanki, P. R.; Srivastava, S.; Ali, M. A.; Srivastava, R. K.; Srivastava, A.; Malhotra, B. *RSC Adv.* **2014**, *4*, 60386.
31. Solanki, P. R.; Ali, M. A.; Agrawal, V. V.; Srivastava, A.; Kotnala, R.; Malhotra, B. *RSC Adv.* **2013**, *3*, 16060.
32. Solanki, P. R.; Patel, M. K.; Ali, M. A.; Malhotra, B. *J. Mater. Chem. B* **2015**, *3*, 6698.
33. Sharma, A.; Baral, D.; Bohidar, H.; Solanki, P. R. *Chem.-Biol. Interactions* **2015**, *238*, 129.
34. Arshak, K.; Adley, C.; Moore, E.; Cunniffe, C.; Campion, M.; Harris, J. *Sensors Actuators B* **2007**, *126*, 226.
35. Chaudhary, A.; Gupta, A.; Mathur, R. B.; Dhakate, S. R. *Adv. Mater. Lett.* **2014**, *5*, 562.
36. Oh, N. W.; Jegal, J.; Lee, K. H. *J. Appl. Polym. Sci.* **2001**, *80*, 2729.
37. Dhand, C.; Das, M.; Sumana, G.; Srivastava, A. K.; Pandey, M. K.; Kim, C. G.; Datta, M.; Malhotra, B. D. *Nanoscale* **2010**, *2*, 747.
38. Mbese, J. Z.; Ajibade, P. A. *Polymers* **2014**, *6*, 2332.
39. Eldin, M. M.; El-Aassar, M.; Elzatahry, A.; Al-Sabah, M. *Arab. J. Chem.* **2014**.
40. Arshad, S. N.; Naraghi, M.; Chasiotis, I. *Carbon* **2011**, *49*, 1710.
41. Kim, I.-C.; Yun, H.-G.; Lee, K.-H. *J. Membr. Sci.* **2002**, *199*, 75.
42. Frey, B. L.; Corn, R. M. *Anal. Chem.* **1996**, *68*, 3187.
43. Taher, A. T.; Khalil, N. A.; Ahmed, E. M. *Arch. Pharm. Res.* **2011**, *34*, 1615.
44. Wang, Y.-Q.; Huang, H.-X.; Li, B.; Li, W.-S. *J. Mater. Chem. A* **2015**, *3*, 5110.
45. Reichman, B.; Bard, A. J.; Laser, D. *J. Electrochem. Soc.* **1980**, *127*, 647.
46. Solanki, P. R.; Kaushik, A.; Ansari, A. A.; Tiwari, A.; Malhotra, B. *Sensors Actuators B* **2009**, *137*, 727.
47. O'Rourke, M.; Duffy, N.; Marco, R. D.; Potter, I. *Membranes* **2011**, *1*, 132.
48. Khan, R.; Dhayal, M. *Biosensors Bioelectron.* **2009**, *24*, 1700.
49. Gupta, P. K.; Khan, Z. H.; Solanki, P. R. *J. Electrochem. Soc. B* **2016**, *163*, 309.
50. Ibupoto, Z. H.; Mitrou, N.; Nikoleli, G. P.; Nikolelis, D. P.; Willander, M.; Psaroudakis, N. *Electroanalysis* **2014**, *26*, 292.
51. Elmlund, L.; Söderberg, P.; Suriyanarayanan, S.; Nicholls, I. A. *Biosensors* **2014**, *4*, 137.
52. Singh, J.; Roychoudhury, A.; Srivastava, M.; Solanki, P. R.; Lee, D. W.; Lee, S. H.; Malhotra, B. *J. Mater. Chem. B* **2013**, *1*, 4493.